The Energy Landscape of 3-Deoxy-D-manno-octulosonate 8-Phosphate Synthase

ARTICLE *in* BIOCHEMISTRY · NOVEMBER 2009

Impact Factor: 3.02 · DOI: 10.1021/bi901341h · Source: PubMed

3 AUTHORS, INCLUDING:

Peng Tao
Southern Methodist University
24 PUBLICATIONS **284** CITATIONS
SEE PROFILE

Domenico L Gatti
Wayne State University
56 PUBLICATIONS **1,536** CITATIONS
SEE PROFILE

BIOCHEMISTRY
including biophysical chemistry & molecular biology
Article

Biochemistry **XXXX,** *XXX,* 000–000 A
DOI: 10.1021/bi901341h

The Energy Landscape of 3-Deoxy-D-*manno*-octulosonate 8-Phosphate Synthase†

Peng Tao,‡,§ Domenico L. Gatti,*,‡ and H. Bernhard Schlegel*,§

‡*Department of Biochemistry and Molecular Biology, Wayne State University School of Medicine, Detroit, Michigan 48201, and* §*Department of Chemistry, Wayne State University, 5101 Cass Avenue, Detroit, Michigan 48202*

Received August 3, 2009; Revised Manuscript Received November 3, 2009

ABSTRACT: 3-Deoxy-D-*manno*-octulosonate 8-phosphate (KDO8P) synthase catalyzes the condensation of arabinose 5-phosphate (A5P) and phosphoenolpyruvate (PEP) to form KDO8P, a key precursor in the biosynthesis of the endotoxin of Gram-negative bacteria. Earlier studies have established that the condensation occurs with a *syn* addition of water to the *si* side of $C2^{PEP}$ and of $C3^{PEP}$ to the *re* side of $C1^{A5P}$. Two stepwise mechanisms have been proposed for this reaction. One involves a transient carbanion intermediate, formed by attack of water or a hydroxide ion on $C2^{PEP}$. The other involves a transient oxocarbenium zwitterionic intermediate, formed by direct attack of $C3^{PEP}$ onto $C1^{A5P}$, followed by reaction of water at C2. In both cases, the transient intermediates are expected to converge to a more stable tetrahedral intermediate, which decays into KDO8P and inorganic phosphate. In this study we calculated the potential energy surfaces (PESs) associated with all possible reaction paths in the active site of KDO8PS: the path involving a *syn* addition of water to the *si* side of $C2^{PEP}$ and of $C3^{PEP}$ to the *re* side of $C1^{A5P}$, with the PEP phosphate group deprotonated, has the lowest energy barrier (~14 kcal/mol) and is strongly exoergonic (reaction energy of −38 kcal/mol). Consistent with the experimental observations, other potential reaction paths, like an *anti* addition of water to the *re* side of $C2^{PEP}$ or addition of $C3^{PEP}$ to the *si* side of $C1^{A5P}$, are associated with much higher barriers. An important new finding of this study is that the lowest energy reaction path does not correspond to either one of the pure stepwise mechanisms proposed formerly but can be described instead as a partially concerted reaction between PEP, A5P, and water. The success in using PESs to reproduce established features of the reaction and to discriminate between different mechanisms suggests that this approach may be of general utility in the study of other enzymatic reactions.

3-Deoxy-D-*manno*-octulosonate (KDO)[1] is an essential constituent of the lipopolysaccharide (LPS, also known as endotoxin) of all Gram-negative bacteria (*1*). Disruption of LPS through inhibition of KDO synthesis leads to severe alteration of normal growth and function (*2*), and without KDO the LPS lacks endotoxin activity (*1*). These observations, and the fact that KDO is present only in Gram-negative bacteria and plants (*3*), suggest that a novel antibiotic strategy could be based on the inhibition of KDO synthesis.

The first step of this synthesis is the condensation of arabinose 5-phosphate (A5P) and phosphoenolpyruvate (PEP) to form KDO 8-phosphate (KDO8P), the phosphorylated precursor of KDO, catalyzed by KDO8P synthase (KDO8PS, EC 2.5.1.55) (*4*). There are two distinct classes of KDO8PSs differing primarily in the requirement, or lack thereof, of a divalent metal ion for activity (*5*, *6*). Crystal structures of metal-free forms from *Escherichia coli* and *Neisseria meningitidis* (*7*−*11*) and of a metal-requiring form from the hyperthermophile *Aquifex aeolicus* (*12*) are available. The structures of the active sites in metallo- and nonmetallo-KDO8PSs are almost identical. In the metalloenzymes, the metal is coordinated by the thiolate of a cysteine, the ε-nitrogen of a histidine, the carboxylate moieties of a glutamic and an aspartic acid, and a water molecule. In nonmetalloenzymes an asparagine replaces the cysteine, and a water molecule (in the same position as the metal-bound water in metalloenzymes) is hydrogen bonded to the asparagine. Naturally occurring nonmetallo-KDO8PSs are as active as their metallo counterparts, and nonmetallosynthases engineered via Cys → Asn substitution (e.g., C11N in *A. aeolicus* KDO8PS) maintain considerable activity (*13*−*15*).

Two stepwise mechanisms have been proposed for the condensation reaction of PEP and A5P to form KDO8P and P_i (Figure 1). One mechanism involves a transient oxocarbenium zwitterionic intermediate (Z_INT), formed by direct attack of $C3^{PEP}$ onto $C1^{A5P}$, followed by reaction of water at $C2^{Z\_INT}$ (lower path in Figure 1). This mechanism was originally proposed for nonmetallo-KDO8PSs (*9*, *16*) but then extended also to the metal forms (*17*−*20*), in which it was thought that the metal ion might play a role as a Lewis acid by coordinating the aldehyde

†This research was supported by U.S. Public Health Service Grant GM69840 to D.L.G., by National Science Foundation Grant CHE0512144 to H.B.S., and by Wayne State University Research Enhancement Program in Computational Biology Grant to D.L.G. and H.B.S. Calculations were conducted on both the Wayne State University Grid (https://www.grid.wayne.edu) and the Teragrid (https://www.teragrid.org).

*Corresponding authors. H.B.S.: tel, 313-577-2562; fax, 313-577-8822; e-mail, hbs@chem.wayne.edu. D.L.G.: tel, 313-993-4238; fax, 313-577-2765; e-mail, dgatti@med.wayne.edu.

[1]Abbreviations: LPS, lipopolysaccharide; KDO, 3-deoxy-D-*manno*-octulosonate; KDO8P, 3-deoxy-D-*manno*-octulosonate 8-phosphate; KDO8PS, 3-deoxy-D-*manno*-octulosonate 8-phosphate synthase; PEP, phosphoenolpyruvate; A5P, arabinose 5-phosphate; C_INT, carbanion intermediate; Z_INT, zwitterionic intermediate; T_INT, tetrahedral intermediate; TS, transition state; HOMO, highest occupied molecular orbitals; LUMO, lowest unoccupied molecular orbitals; NBO, natural bond orbital; rmsd, root-mean-square deviation; QM, quantum mechanics; MM, molecular mechanics; MD, molecular dynamics; ps, picosecond; PES, potential energy surface.

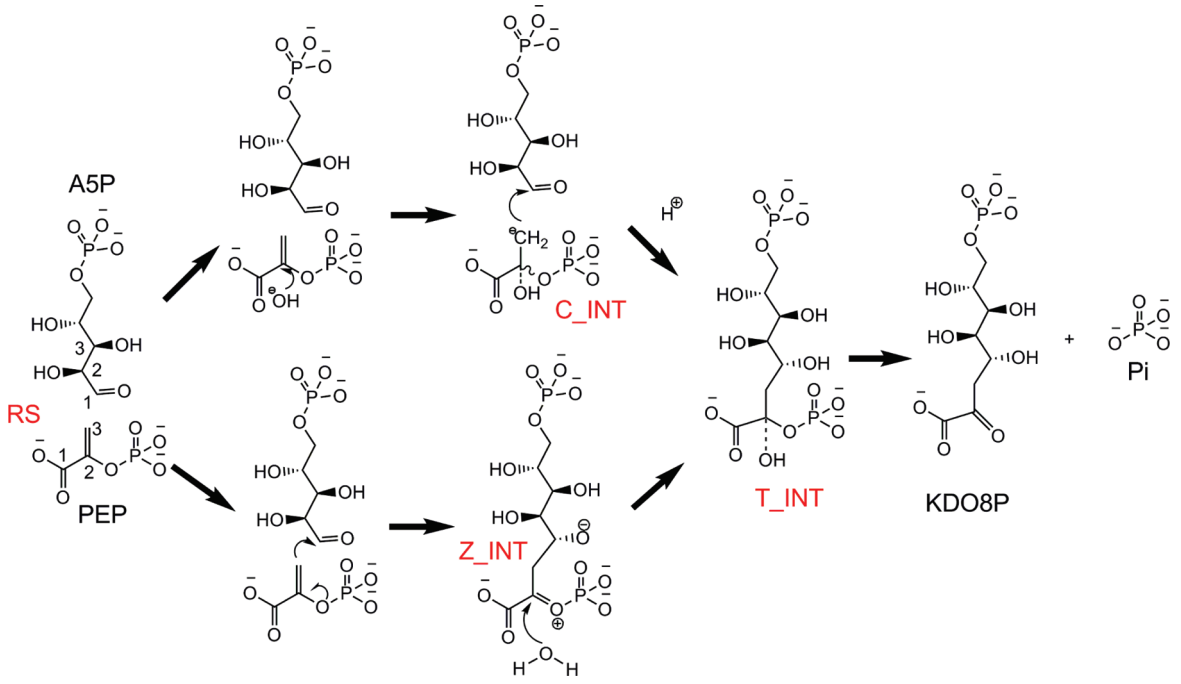

FIGURE 1: Proposed mechanisms for PEP and A5P condensation.

group of A5P. The resulting polarization of the aldehyde carbonyl would facilitate the nucleophilic attack by C3 of PEP to the aldehyde of A5P. Interestingly, this idea found support in an earlier paper by Du et al. (*21*) in which solution synthesis of KDO8P was reported to occur by intramolecular addition of the enolpyruvate double bond to the aldehyde carbonyl of a model compound at pH 5.0 in the presence of Zn^{2+} ions. Also in this reaction the metal was believed to act primarily as a Lewis acid by activating the aldehyde carbonyl. However, structural studies of *A. aeolicus* Cd^{2+} KDO8PS in complex with both PEP and A5P did not support this suggestion. In this enzyme the C2-OH (not the carbonyl oxygen of the aldehyde) of A5P was found to interact indirectly with the active site metal via a water molecule located on the *si* side of PEP (*12*). On this basis, a different mechanism was proposed for metallo-KDO8PSs (upper path in Figure 1), which involved a transient carbanion intermediate (C_INT), formed by attack of water or a hydroxide ion on $C2^{PEP}$ (*22*, *23*). This mechanism relied on the assumption that the metal would favor the deprotonation of the coordinated water to a hydroxide ion, which would be a good nucleophile for attack on $C2^{PEP}$. The ensuing carbanion at $C3^{PEP}$ would then facilitate attack of $C3^{PEP}$ to $C1^{A5P}$. In both mechanisms, the transient intermediates (C_INT or Z_INT) are expected to converge to a more stable tetrahedral intermediate (T_INT), which decays into KDO8P and P_i (Figure 1), as originally proposed by Hedstrom and Abeles (*24*). T_INT has been observed by electrospray ionization mass spectrometry (*25*) and also in the crystal structure of the C11N/S235P/Q237A triple mutant of *A. aeolicus* KDO8PS (*26*). The configuration of the $C2^{T\_INT}$ chiral center in one of the active sites visible in this structure suggests that water attacks the *si* side of $C2^{PEP}$ or $C2^{Z\_INT}$ such that the overall condensation reaction would correspond to a *syn* addition of water and A5P to the C2 and C3 carbons of PEP. However, in the other active sites of the same crystal structure a water molecule is not visible on the *si* side of PEP when A5P is also bound, making it difficult to explain how the *syn* addition might have occurred. Furthermore, in the crystal structures of all KDO8PSs there is another water molecule on the *re* side of $C2^{PEP}$ (*26*), which would lead to the arguably more stable *anti* addition of water and A5P to the C2−C3 double bond of PEP. In an initial effort to discriminate between *syn* and *anti* addition Howe et al. (*23*) have used Hartree−Fock theory to calculate in the gas phase the electron density, highest occupied molecular orbitals (HOMO), and lowest unoccupied molecular orbitals (LUMO) for the energy-minimized unbound conformation of PEP and the enzyme-bound conformations of PEP in the *A. aeolicus* KDO8PS−PEP binary complex and the KDO8PS−PEP−A5P ternary complex. The bending of PEP from planarity in the active site of the ternary complex was found to increase the positive charge on the *si* face of $C2^{PEP}$. These results are very encouraging and suggest that a conclusive explanation of why one type of attack is preferred over the other might be obtained by exploring the electronic properties of the substrates in the condensed phase of the active site. Earlier evidence also indicates that the condensation of PEP and A5P is stereospecific, involving the addition of the *si* face of $C3^{PEP}$ to the *re* face of the A5P carbonyl (*27*, *28*). However, the crystal structures show that there are no obstacles in the active site to the rotation of the A5P carbonyl group. Molecular dynamics simulations likewise show two equally represented orientations of the A5P carbonyl group related by a rotation of 180° around $C1-C2^{A5P}$ (see Supporting Information in this study), which would lead to an attack by $C3^{PEP}$ onto the *re* or *si* side of $C1^{A5P}$ with equal probability. Also in this case the reason why one type of addition is preferred over the other may lie in the electronic properties of A5P in the active site.

In this study we explored the reaction of KDO8P synthesis in the C11N form of *A. aeolicus* KDO8PS (which under all respects can be considered as a nonmetal variant of the *A. aeolicus* enzyme) with a systematic construction by quantum mechanics/molecular mechanics (QM/MM) calculations of the potential energy surfaces (PESs) corresponding to all possible reaction paths. The successful discrimination between different postulated mechanisms of KDO8P synthesis accomplished with this strategy

and the correspondence found with established chemical features of the reaction suggest that a similar approach may also be effective in the analysis of other complex enzymatic reactions.

COMPUTATIONAL METHODS

The X-ray structure of the C11N form of *A. aeolicus* KDO8PS (PDB entry 2NWS) was used as the starting point for the study. After inclusion of additional solvent molecules (represented by the TIP3P model (*29*)) inside a box, with a minimum distance of 12 Å between the protein complex and the box's surface, the system was relaxed with Amber v.9, using the all-atom force field ff03 of Duan et al. (*30*), first through 20000 steps of conjugate gradient energy minimization and then with a short molecular dynamics (MD) run of 40 ps (ps) under periodic boundary conditions, using the SHAKE method (*31*) to constrain the length of all covalent bonds with hydrogen. At this point, in order to facilitate the computation, only the water molecules within 6 Å of the protein or within 12 Å of A5P or PEP were kept for the QM/MM calculations.

A two-layer ONIOM method (*32*−*34*) was used for all the QM/MM calculations. A5P, PEP, and a water molecule were included in the QM region (38 atoms) and were described at the B3LYP/3-21G level of density functional theory. The rest of the system was described by molecular mechanics using the *parm96* parameters of the Amber force field. A mechanical embedding scheme was used for geometry optimization (electrostatic interactions between the QM and MM regions are handled by MM in this approach). PESs were constructed using QM/MM calculations on a two-dimensional grid employing the forming C−O bond between the attacking water and PEP and the C−C bond between PEP and A5P as reaction coordinates. Approximately 200 points were obtained for each surface by constraining the two grid coordinates and minimizing the energy with respect to the remaining parameters. For each point on the surfaces, the geometry was optimized with the quadratically coupled QM/MM optimizer implemented in the development version of the Gaussian package (Gaussian Inc.). QM/MM energies were then calculated for each point at the B3LYP/6-31+G(d,p) level of theory for the QM part using an electronic embedding scheme (*34*). Analytical forms of the PESs were obtained with Mathematica 7 (Wolfram Research, Inc.) by linear least-squares fitting using a polynomial with terms up to eighth order in the coordinates. The analytical PESs were used to identify the transition states (TSs) and to generate minimum energy reaction paths from reactant to product on the surfaces using the steepest descent method. The structure of TS1 on PES I was further refined by the quadratic synchronous transit method (QST) (*35*−*37*) utilizing two points of the surface on opposite sides of the TS.

In order to generate the PES of the uncatalyzed condensation reaction in solution, PEP, A5P, and the reacting water molecule (corresponding to the components of the RS state of PES I) were initially immersed in a box (60 Å × 60 Å × 60 Å) of explicit TIP3P water molecules. After an initial geometry optimization, the system was equilibrated with a short MD run for 40 ps under periodic boundary conditions and SHAKE constraints. At this point all of the solvent molecules farther than 26 Å from $C1^{A5P}$ were discarded, and the coordinates of those farther than 20 Å from $C1^{A5P}$ were frozen. During the following relaxed coordinate scan, PEP, A5P, and the water involved in the reaction were treated by QM, while all of the other waters were treated by MM.

The reorganization energy of the reaction on the PESs I and I_{wat} was computed by extracting the atoms of the solute (PEP, A5P, and the reacting water) from the product state of the ensemble (solute + environment) and transferring them into the reactant state of the environment alone. In the case of the enzymatic reaction, the environment was represented by the protein and all protein-bound water molecules not involved in catalysis; in the case of the reaction in solution the environment was represented by all of the other water molecules not directly involved in the reaction. At this point, the coordinates of the solute were frozen, and the environment was allowed to relax. The energy difference associated with such relaxation provides an estimate of the reorganization energy (*38*, *39*).

Atomic charges of the RS and TS1 states in water and in the active site were calculated with a natural bond orbital (NBO) analysis of the wave function of the QM region using NBO 5.0 (*40*).

RESULTS

The X-ray structure of the C11N variant form of *A. aeolicus* KDO8PS (PDB entry 2NWS) was chosen as the starting point for the study. This is the only nonmetal form of KDO8PS for which a high-resolution structure containing both PEP and A5P in the active site is available (*26*). We constructed a series of PESs (Figure 2) based on QM/MM calculations, corresponding to both *syn* and *anti* additions of water and A5P to the double bond of PEP. The distances between the oxygen of the attacking water O^{WAT} and $C2^{PEP}$ (CO) and between $C3^{PEP}$ and $C1^{A5P}$ (CC) were defined as the reaction coordinates. Four different mechanisms were investigated in detail corresponding to water attack on the *si* or the *re* side of $C2^{PEP}$ and to $C3^{PEP}$ attack on the *re* or the *si* side of $C1^{A5P}$. Since it has been suggested (*41*) that the ionization state of the phosphate moiety of PEP may affect catalysis, for each mechanism, PESs were calculated with the PEP phosphate either doubly or singly ionized. In each PES of Figure 2 the right corner represents the reactant state (RS), the top corner represents C_INT + A5P, the lower corner represents Z_INT + WAT, and the left corner represents the product state (PS), which in this case is T_INT. Colors on the PESs designate proton movements between the attacking water molecule, the phosphate group oxygen of PEP, and the carbonyl oxygen of A5P. Qualitatively, green indicates that both protons are with the water molecule, blue that one proton approaches the A5P carbonyl oxygen, and red that one proton approaches the PEP phosphate. Colors on the projected contours below the PESs reflect energy levels, with darker shades of blue corresponding to lower energy.

Water Attacks the si Side of $C2^{PEP}$, and $C3^{PEP}$ Attacks the re Side of $C1^{A5P}$. In the first simulation (PES I, Figure 2A) the phosphate group of PEP is completely deprotonated at the RS, and water forms hydrogen bonds with this phosphate group and with $C3-OH^{A5P}$. Formation of C_INT + A5P from RS is endothermic (reaction energy ∼ 40 kcal/mol) and associated with transfer of one proton from water to the phosphate group of PEP. Formation of Z_INT + WAT from RS is exothermic (reaction energy ∼ −11 kcal/mol): in this state the bridging oxygen of Z_INT displays one elongated PO bond (1.86 Å) and one shortened CO bond (1.29 Å) (Figure 3). Formation of T_INT from RS is very exothermic (reaction energy ∼−38 kcal/mol, Table 1): in this state, $C2-OH^{T\_INT}$, which originates from the water molecule that attacks $C2^{PEP}$, donates a hydrogen

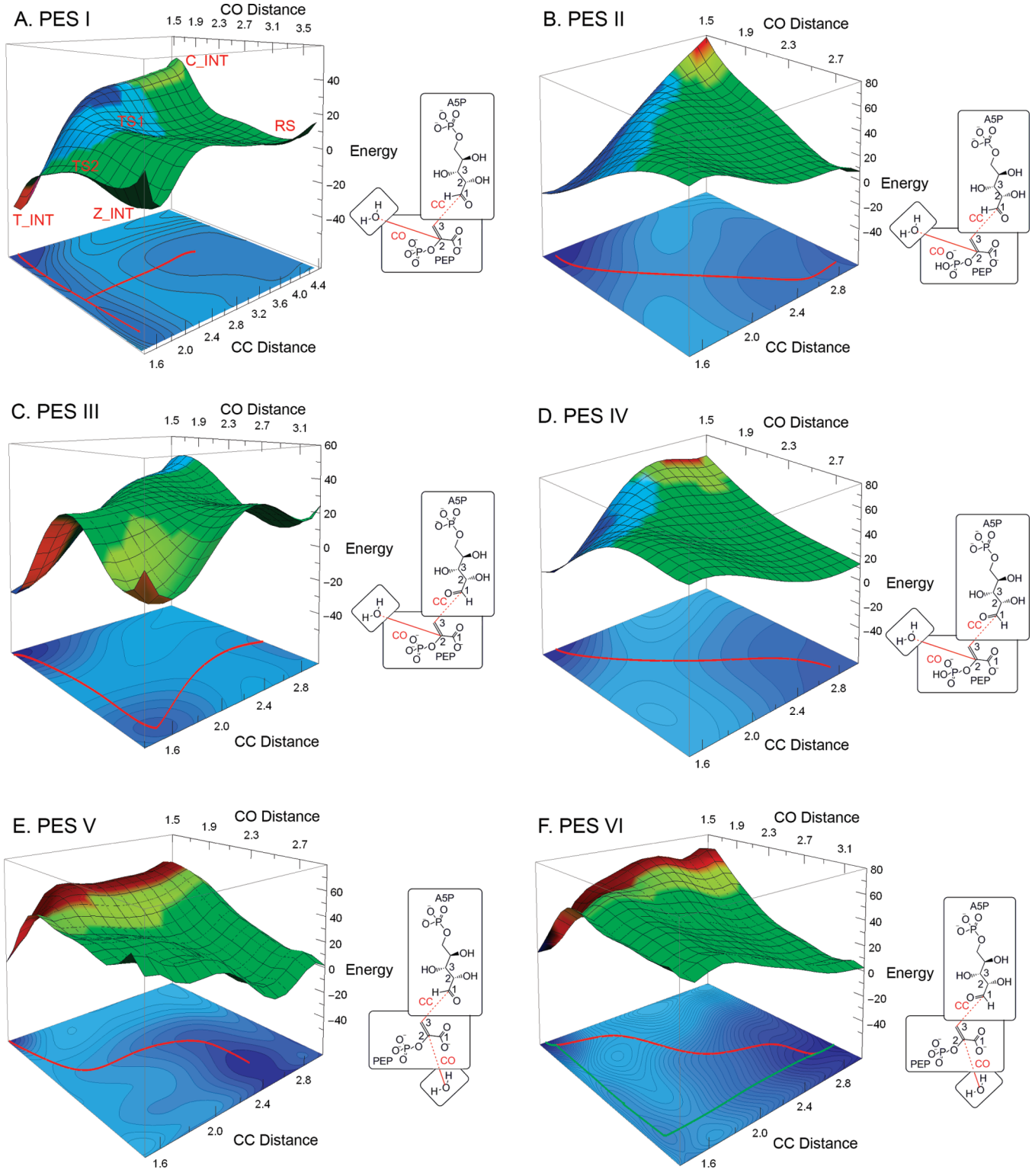

FIGURE 2: (A) PES I, reaction in which O^{WAT} attacks the *si* side of $C2^{PEP}$ and $C3^{PEP}$ attacks the *re* side of $C1^{A5P}$; PEP phosphate is deprotonated. (B) PES II, same as (A) but with PEP phosphate partially protonated. (C) PES III, reaction in which O^{WAT} attacks the *si* side of $C2^{PEP}$ and $C3^{PEP}$ attacks the *si* side of $C1^{A5P}$; PEP phosphate is deprotonated. (D) PES IV, same as (C) but with PEP phosphate partially protonated. (E) PES V, reaction in which O^{WAT} attacks the *re* side of $C2^{PEP}$ and $C3^{PEP}$ attacks the *re* side of $C1^{A5P}$; PEP phosphate is deprotonated. (F) PES VI, reaction in which O^{WAT} attacks the *re* side of $C2^{PEP}$ and $C3^{PEP}$ attacks the *si* side of $C1^{A5P}$; PEP phosphate is deprotonated. CC and CO distances are in Å; energies are in kcal/mol. Colors on the PESs represent in a qualitative way proton movements along the reaction path: green for proton on O^{WAT}, blue for proton nearing $O1^{A5P}$, and red for proton nearing PEP phosphate oxygen. Colors on the projected contours below the PESs reflect energy levels, with darker shades of blue corresponding to lower energy.

bond to the carbonyl oxygen of A5P, while the other proton from water has migrated to the PEP phosphate.

A reaction path on the analytical PES I (Figure 2A, red line; see also Supporting Information Figure S2 for a different view of this PES) goes through two consecutive TSs. At the TS1, which corresponds to a barrier of ~14 kcal/mol, the CO and CC distances are 2.61 and 2.16 Å, respectively (Figure 3); the two water hydrogens are ~1.8 Å from the carbonyl oxygen of A5P

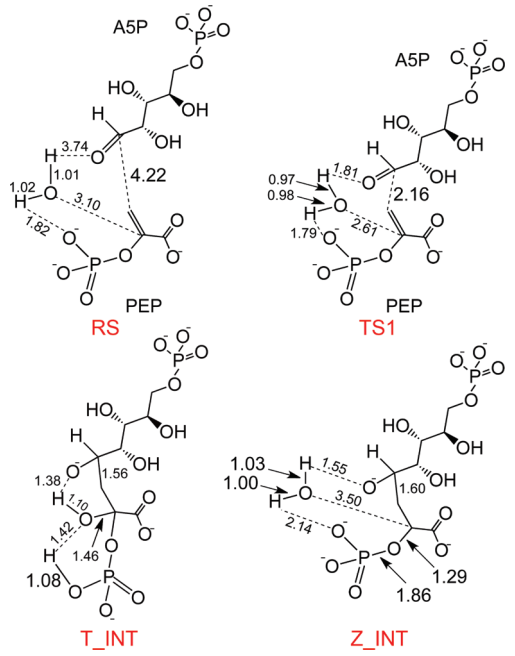

FIGURE 3: Atom pair distances (in Å) for key structures on PES I.

Table 1: Reaction Energies[a] in KDO8PS PESs

PES	water attack on $C2^{PEP}$ side	PEP attack on $C1^{A5P}$ side	PEP charges	TS1	Z_INT	TS2	T_INT
I	*si*	*re*	−3	14	−11	−5	−38
I_{wat}	*si*	*re*	−3	38	4	10	−16
II	*si*	*re*	−2	41			−19
III	*si*	*si*	−3	25	−10	25	−27
IV	*si*	*si*	−2	47			−4
V	*re*	*re*	−3	44			−2
VI	*re*	*si*	−3	44	38	48	3

[a]Reaction energies (kcal/mol) were calculated at the ONIOM(B3LYP/6-31+G(d,p):AMBER) level of theory.

and a phosphate oxygen of PEP, respectively. The path from TS1 leads to TS2, in which the CO bond remains around 2.6 Å and the CC bond is already fully formed (1.6 Å). This is a bifurcation point from which the reaction can proceed to Z_INT (corresponding to a strict stepwise mechanism) or to T_INT (a sequential mechanism without a separate intermediate). Since the barrier between Z_INT and T_INT (~6 kcal/mol) is much lower than the first barrier between RS and Z_INT (~14 kcal/mol), and T_INT is lower in energy than Z_INT (~27 kcal/mol), the system is not expected to be significantly populated in the pure Z_INT state. Overall, PES I reflects a mainly stepwise mechanism, in which the rate-limiting step is clearly the formation of the CC bond between PEP and A5P, with some character of a concerted reaction between PEP, A5P, and water.

PES II (Figure 2B) is the analogue of PES I but with the PEP phosphate partially protonated. The reaction path (red line) corresponds to a concerted attack of O^{WAT} on $C2^{PEP}$ and of $C3^{PEP}$ on $C1^{A5P}$. At the TS, the CO bond (2.2 Å) between $C2^{PEP}$ and O^{WAT} and the CC bond (2.0 Å) between $C3^{PEP}$ and $C1^{A5P}$ are partially formed. The attacking water forms hydrogen bonds with both the phosphate group of PEP and the A5P carbonyl group. In the T_INT complex (left corner of the PES) a proton has migrated from this water to the carbonyl oxygen of A5P (which becomes $C4{-}OH^{T\_INT}$). Accordingly, the surface color changes from green to blue in this region. The overall reaction is less exothermic than that of PES I (~−19 kcal/mol), and the barrier is significantly higher (~41 kcal/mol). Unlike in PES I, Z_INT (lower corner of the PES) is very high in energy (~50 kcal/mol) compared to the T_INT and TS complexes, and a reaction path through it is not possible. C_INT (upper corner of the PES) is the intermediate with the highest energy (~78 kcal/mol).

Water Attacks the si Side of $C2^{PEP}$, and $C3^{PEP}$ Attacks the si Side of $C1^{A5P}$. In the first simulation (PES III, Figure 2C) the phosphate group of PEP is completely deprotonated, and water forms hydrogen bonds with both the phosphate and the carboxylate groups of PEP. In the TS the attacking water forms hydrogen bonds with the PEP phosphate and remotely with the A5P carbonyl oxygen. The barrier (25 kcal/mol) to T_INT is about 10 kcal/mol higher than the corresponding barrier for attacking on the *re* side of $C1^{A5P}$ (PES I). The reaction is exothermic (−27 kcal/mol) but less than in the reaction path on PES I. The energy of C_INT is higher than that of T_INT and comparable to that of TS. The barrier from RS to Z_INT is 25 kcal/mol, and Z_INT is lower in energy than RS, but contrary to PES I, transformation of Z_INT into T_INT has a very high barrier (~35 kcal/mol). The reaction barriers from RS to T_INT are much higher in this PES, providing an explanation for why the condensation reaction does not proceed with an attack from $C3^{PEP}$ onto the *si* side of $C1^{A5P}$.

PES IV (Figure 2D) is the counterpart of PES III with the PEP phosphate partially protonated. The reaction from RS to T_INT is much less exothermic than in PES III (−4 kcal/mol compared to −27 kcal/mol) and the barrier much higher (47 kcal/mol compared to 25 kcal/mol). Both C_INT and Z_INT have energies higher than the TS on the surface.

Water Attacks the re Side of $C2^{PEP}$. This reaction corresponds to an *anti* addition of water and A5P to the double bond of PEP, and the C2 chiral center of T_INT has the *S* configuration (versus *R* when water attacks the *si* side of $C2^{PEP}$). In the first simulation (PES V, Figure 2E) $C3^{PEP}$ attacks the *re* side of $C1^{A5P}$ as in PESs I and II. The most probable reaction path corresponds to a one-step reaction with concerted formation of the CO and CC bonds. The reaction energy from RS to T_INT is only −2 kcal/mol, and the reaction barrier is approximately 44 kcal/mol. Since the A5P carbonyl group and the attacking water are located on opposite sides of the PEP C=C double bond plane, the water proton can only migrate to the phosphate (as indicated by the red shading on the surface).

In the second simulation (PES VI, Figure 2F) $C3^{PEP}$ attacks the *si* side of $C1^{A5P}$ as in PESs III and IV. Conversion of RS into T_INT is endothermic (3 kcal/mol). Two potential reaction paths can be recognized on the surface: one path (red line) corresponds to a concerted formation of both the CO and CC bonds and has a barrier ca. 55 kcal/mol. The hydroxyl group from the attacking water forms a hydrogen bond with the adjacent phosphate group (as indicated by the red shading on the surface). The other path (green line) corresponds to a stepwise reaction in which the CC bond is formed first (RS to Z_INT barrier = 44 kcal/mol), followed by the CO bond (Z_INT to T_INT barrier = 10 kcal/mol). To recapitulate, the high barriers of PESs V and VI exclude a mechanism in which water attacks the *re* side of $C2^{PEP}$.

DISCUSSION

Among the various PESs calculated in this study, the lowest energy reaction path from RS (PEP + A5P + H_2O) to T_INT

(the experimentally observed intermediate) was observed on PES I, which describes a *syn* addition of water to the *si* side of $C2^{PEP}$ and of $C3^{PEP}$ to the *re* side of $C1^{A5P}$ when the phosphate group of PEP is deprotonated. The calculated barrier and reaction energy for this path are ~14 and −38 kcal/mol, respectively. Other possible paths, like an *anti* addition of water to the *re* side of $C2^{PEP}$ or addition of $C3^{PEP}$ to the *si* side of $C1^{A5P}$, are associated with much higher energy barriers (PESs III, V, VI). These results are consistent with established features of the reaction (*26*−*28*) and thus confirm the validity of the calculations. The new finding of this study is that the lowest energy path to the formation of T_INT does not correspond to either of the pure stepwise processes described in Figure 1 but corresponds instead to a partially concerted reaction between PEP, A5P, and water in the enzyme active site.

In the formalism of classical transition-state theory (TST) (*42*, *43*), the rate constant of an enzymatic reaction can be approximated as

$$k_{cat} \approx \kappa k_{TST} \quad k_{TST} \approx (k_B T/h) \exp(-\Delta G^{\ddagger}/RT)$$

where k_B is the Boltzmann constant, R is the gas constant, T is the absolute temperature, and h is Planck's constant. The exponential factor in this expression simply represents the probability of finding the reactant at the TS. Additional dynamical effects that may contribute to enzyme catalysis are usually combined in the transmission coefficient κ, which incorporates both the probability that a system arriving at the TS from the reactant side of the barrier will end up on the product side and the average number of times that a productive trajectory passes back and forth across the TS before ending up permanently on the product side. For most biological reactions that have been studied in detail κ was found to be between 0.1 and 1.0 for both the enzymatic reaction and the corresponding reaction in solution (*44*−*47*). We have used a value of 0.6 as the average of the values found for yeast enolase and triose phosphate isomerase, which are structurally similar to KDO8PS. The activation barrier $\Delta G^{\ddagger}_{cat}$ generally includes differences in entropy in addition to enthalpy. However, the PESs derived from our QM/MM relaxed scans do not include entropic contributions. In an early analysis of entropic effects, Page and Jencks (*48*, *49*) assumed that the loss of rotational and translational degrees of freedom associated with a bimolecular enzymatic reaction occurs during the formation of the enzyme−substrate (ES) complex and that no additional change in entropy ($\Delta S^{\ddagger}_{cat} \approx 0$) occurs during the progression of the ES complex into the TS. More recently, Snider et al. (*50*) found that in cytidine deaminase $T\Delta S^{\ddagger}_{cat} \approx 0.9$ kcal/mol and that most of the entropy changes occur during substrate binding ($T\Delta S_{bind} \approx -7.6$ kcal/mol). However, Villa et al. (*51*) calculated that for a peptide hydrolysis by subtilisin $T\Delta S^{\ddagger}_{cat} \approx -2.5$ kcal/mol and that the corresponding contribution to the TS entropy in a cage of water of the same size as the active site is of comparable magnitude (that is, $T\Delta S^{\ddagger}_{cage} \approx -2.6$ kcal/mol). The reader is referred to the relevant literature (*38*, *39*, *52*) for a detailed discussion of the concept of "cage" and its application to the analysis of reactions in solution; a synoptic explanation is also provided in the Supporting Information. Thus, while the assumption that $\Delta S^{\ddagger}_{cat} \approx 0$ is certainly incorrect, entropic contributions to $\Delta G^{\ddagger}_{cat}$ probably do not exceed 3 kcal/mol in most enzymatic reactions and are not significantly different in the enzyme active site with respect to the same reaction in solution.

In previous studies we have reported k_{cat} values around 0.2−0.6 s^{-1} at 40 °C for the rate of condensation of PEP and A5P to T_INT in several forms of *A. aeolicus* KDO8PS (*26*, *53*). The reaction mechanism corresponding to PES I ($\Delta G^{\ddagger}_{cat} = \Delta H^{\ddagger}_{cat} - T\Delta S^{\ddagger}_{cat} = 14 + \sim 3$ kcal/mol) is expected to yield a $k_{cat} \approx \kappa k_{TST} \approx 5.4\ s^{-1}$, a reasonable match to the experimental value. This fact, and the significant structural similarity between the experimentally observed and the calculated T_INT (rmsd of only 1.4 Å), lends validity to the mechanistic model represented by PES I.

For comparison with the enzymatic system, the uncatalyzed condensation reaction in solution (corresponding to the enzyme-catalyzed reaction of PES I) was calculated inside a spherical region of 26 Å radius filled with water molecules (PES I_{wat}, Figure 4; see also Table 1). The reaction in solution is less exothermic (−16 kcal/mol) than in the enzyme and proceeds preferentially in a stepwise manner first with formation of a CC bond between $C3^{PEP}$ and $C1^{A5P}$ with very high barrier (~38 kcal/mol) and then with formation of a bond between O^{WAT} and

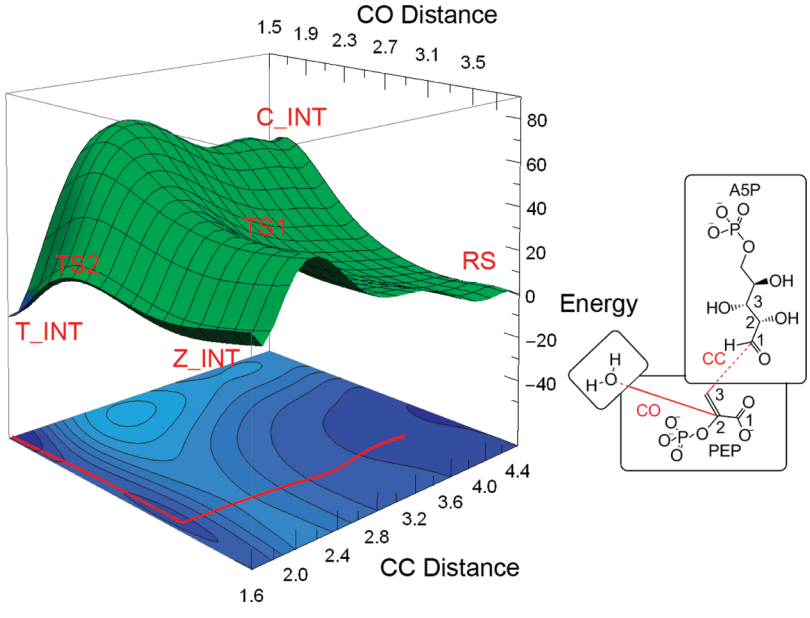

FIGURE 4: PES I_{WAT}, reaction in solution in which O^{WAT} attacks the *si* side of $C2^{PEP}$ and $C3^{PEP}$ attacks the *re* side of $C1^{A5P}$; PEP phosphate is deprotonated. Abbreviations and colors as in Figure 2.

Table 2: Atom Charges at the Energy Minimum of the RS State and at the TS1 State in Water (PES I_{wat}) and in the Active Site (PES I)[a]

		RS minimum		RS Δcharge	TS1		TS1 Δcharge
		water	active site	active site − water	water	active site	active site − water
PEP	O1	−0.7799	−0.7957	−0.0158	−0.7671	−0.7585	0.0086
	O2	−0.8698	−0.8617	0.0081	−0.8564	−0.8846	−0.0282
	C1	0.7692	0.7676	−0.0016	0.7569	0.7835	0.0266
	C2	*0.2472*	*0.1830*	***−0.0642***	*0.3907*	*0.4485*	***0.0578***
	C3	*−0.6158*	*−0.5363*	***0.0795***	*−0.6350*	*−0.6327*	***0.0023***
	O4P	*−0.8356*	*−0.8665*	***−0.0309***	*−0.7626*	*−0.7882*	***−0.0256***
	P	2.5205	2.5014	−0.0191	2.5198	2.5078	−0.0120
	O1P	−1.2408	−1.2051	0.0357	−1.2596	−1.2470	0.0126
	O2P	−1.2476	−1.2674	−0.0198	−1.2374	−1.2594	−0.0220
	O3P	−1.2738	−1.2502	0.0236	−1.2672	−1.2466	0.0206
A5P	***O1***	*−0.6503*	*−0.7378*	***−0.0875***	*−0.6821*	*−0.7682*	***−0.0861***
	C1	*0.4044*	*0.3857*	***−0.0187***	*0.3030*	*0.2846*	***−0.0184***
	C2	−0.0202	−0.0106	0.0096	0.0078	0.0081	0.0003
	O2	−0.8421	−0.8016	0.0405	−0.8055	−0.7939	0.0116
	C3	0.0562	0.0515	−0.0047	0.0449	0.0588	0.0139
	O3	−0.8143	−0.8252	−0.0109	−0.7725	−0.8006	−0.0281
	C4	0.0387	0.0345	−0.0042	0.0372	0.0211	−0.0161
	O4	−0.7902	−0.8420	−0.0518	−0.8112	−0.8383	−0.0271
	C5	−0.1263	−0.1081	0.0182	−0.1195	−0.1249	−0.0054
	O4P	−0.9014	−0.8766	0.0248	−0.9062	−0.8698	0.0364
	P	2.5356	2.4907	−0.0449	2.5241	2.5090	−0.0151
	O1P	−1.2742	−1.3021	−0.0279	−1.2892	−1.3273	−0.0381
	O2P	−1.2565	−1.3304	−0.0739	−1.2948	−1.3449	−0.0501
	O3P	−1.2666	−1.2405	0.0261	−1.2753	−1.2369	0.0384
WAT	***O***	*−1.0582*	*−0.9369*	***0.1213***	*−1.0898*	*−0.9811*	***0.1087***

[a]Atomic charges were calculated from a natural bond orbital (NBO) (*40*) analysis of the wave function of the quantum atoms. Rows of atoms expected to be involved in the condensation reaction are italicized. O4P is the carbon−phosphate bridging oxygen in both PEP and A5P.

$C2^{PEP}$ with lower barrier (~6 kcal/mol). The calculated value for the rate constant of this reaction (assuming $\Delta G^{\ddagger}_{cage} = \Delta H^{\ddagger}_{cage} - T\Delta S^{\ddagger}_{cage}$ = 38 + ~3 kcal/mol) is ~1.7×10^{-16} s^{-1}, based on which the rate enhancement in the enzyme-catalyzed reaction is estimated to be approximately 10^{16}-fold. This remarkable achievement appears to be accomplished primarily thanks to the fact that the environment provided by the KDO8PS active site is rather "stiff" compared to the environment provided by a water solution. In fact, the reorganization energy of the enzyme (estimated by placing the product state of the solute into the reactant state of the enzyme, and letting the enzyme relax around the frozen solute; see Computational Methods) associated with the progression from RS to T_INT on PES I was determined to be only 40 kcal/mol, compared to 159 kcal/mol for the same reaction occurring in solution on PES I_{wat} (Table 1, Figure 4). One possible interpretation of this result is that the folded enzyme provides a dipolar environment that in the reactant state is already partially oriented to stabilize the charge distribution of the TS. Therefore, little additional reorientation occurs when the reaction progresses to the TS (*38*, *39*, *54*). Instead, although the interaction energy of the substrates with the solvent atoms is equal or even larger than the corresponding interaction energy with the protein atoms, reorienting the solvent polar environment toward the TS during the reaction in water requires a much larger energy investment (a price already paid by the enzyme during the folding process). The protein stiffness can be recognized in the comparable degree of polarization (at the energy minimum of the RS state and at TS1) of the charges of some key atoms involved in the reaction (e.g., $O4P^{PEP}$, $O1^{A5P}$, $C1^{A5P}$, O^{WAT}; Table 2) with respect to the charges in water. Clearly, there are also cases in which the charge polarization produced by the enzyme at the TS1 is quite different from that at the RS (e.g., $C2^{PEP}$, $C3^{PEP}$; Table 2), suggesting a more significant degree of reorganization around those atoms. It is worth noting that if one considers a valence bond (VB) representation of the reaction as a mixture of diabatic states corresponding to reactant and product, it can be seen that the reorganization energy λ is approximately 4 times the value of the activation energy $\Delta G^{\ddagger}$ (*39*, *52*) (see also Supporting Information for a brief explanation). Thus, the values of the reorganization energies calculated for the reaction in the enzyme and in solution are consistent with the activation energies derived from PES I and PES I_{wat}.

A key finding of this study is that the rate-limiting step of the condensation reaction (as identified on PES I) is the formation of a CC bond between PEP and A5P (TS1, Figure 2A, Table 1). This step is immediately followed by the formation of a CO bond between PEP and water (TS2, Figure 2A, Table 1). One might note that while TS2 is a real transition state for the uncatalyzed reaction in water (Figure 4), in the enzymatic reaction it is associated with a small activation barrier only along the path from Z_INT to T_INT, as the path from TS1 to T_INT through TS2 is all downhill. Thus, overall, the two closely related TSs reflect a more clearly defined stepwise reaction in solution and a partially concerted reaction between PEP, A5P, and water in the enzyme active site. However, the ridge of PES I on which TS1 resides is long and shallow, and thus it is possible for other thermally activated states to overcome the barrier. In general, it appears that a pure stepwise reaction in which Z_INT is a true stable intermediate that subsequently reacts with water (Figures 1 and 2A) might be favored in a slightly different configuration of the enzyme. This observation supports the view proposed by Benkovic et al. (*55*), according to which enzyme catalysis is

associated with an ensemble of conformations, leading to parallel reaction paths, such that the dominant pathways that are ultimately followed may change with the reaction conditions. This means that, in situations such as that represented by the shallow PES I of the condensation reaction catalyzed by KDO8PS, successful inhibition of a key enzyme in a metabolic pathway may require a mixture of transition state analogues or a combination with agents capable of collapsing the conformational ensemble into a few and ultimately only one active configuration. This observation highlights the importance of computing the PESs of all possible reaction paths as an effective avenue to achieve information about the energy landscape of enzymatic reactions that is unattainable by other means.

ACKNOWLEDGMENT

We thank Dr. Sharon H. Ackerman for careful reading of the manuscript and helpful discussions.

SUPPORTING INFORMATION AVAILABLE

Molecular dynamics of KDO8PS, Figure S1, additional references; Figure S2, different viewpoint of PES I; Figure S3, brief description of the "cage" concept as referred to $\Delta G^{\ddagger}_{cage}$; Figure S4, relationship between reorganization energy and $\Delta G^{\ddagger}$. This material is available free of charge via the Internet at http://pubs.acs.org.

REFERENCES

1. Raetz, C. R., and Whitfield, C. (2002) Lipopolysaccharide endotoxins. *Annu. Rev. Biochem. 71*, 635–700.
2. Rick, P. D., and Young, D. A. (1982) Isolation and characterization of a temperature-sensitive lethal mutant of *Salmonella typhimurium* that is conditionally defective in 3-deoxy-D-manno-octulosonate-8-phosphate synthesis. *J. Bacteriol. 150*, 447–455.
3. Doong, R. L., Ahmad, S., and Jensen, R. A. (1991) *Plant Cell Environ. 14*, 113–120.
4. Levin, D. H., and Racker, E. (1959) Condensation of arabinose 5-phosphate and phosphorylenol pyruvate by 2-keto-3-deoxy-phosphooctonic acid synthetase. *J. Biol. Chem. 234*, 2532–2539.
5. Birck, M. R., and Woodard, R. W. (2001) *Aquifex aeolicus* 3-Deoxy-D-manno-2-octulosonic acid 8-phosphate synthase: a new class of KDO 8-P synthase? *J. Mol. Evol. 52*, 205–214.
6. Duewel, H. S., and Woodard, R. W. (2000) A metal bridge between two enzyme families. 3-Deoxy-D-manno-octulosonate 8-phosphate synthase from *Aquifex aeolicus* requires a divalent metal for activity. *J. Biol. Chem. 275*, 22824–22831.
7. Radaev, S., Dastidar, P., Patel, M., Woodard, R. W., and Gatti, D. L. (2000) Structure and mechanism of 3-deoxy-D-manno-octulosonate 8-phosphate synthase. *J. Biol. Chem. 275*, 9476–9484.
8. Wagner, T., Kretsinger, R. H., Bauerle, R., and Tolbert, W. D. (2000) 3-Deoxy-D-manno-octulosonate-8-phosphate synthase from *Escherichia coli*. Model of binding of phosphoenolpyruvate and D-arabinose-5-phosphate. *J. Mol. Biol. 301*, 233–238.
9. Asojo, O., Friedman, J., Adir, N., Belakhov, V., Shoham, Y., and Baasov, T. (2001) Crystal structures of KDOP synthase in its binary complexes with the substrate phosphoenolpyruvate and with a mechanism-based inhibitor. *Biochemistry 40*, 6326–6334.
10. Vainer, R., Belakhov, V., Rabkin, E., Baasov, T., and Adir, N. (2005) Crystal structures of *Escherichia coli* KDO8P synthase complexes reveal the source of catalytic irreversibility. *J. Mol. Biol. 351*, 641–652.
11. Cochrane, F. C., Cookson, T. V., Jameson, G. B., and Parker, E. J. (2009) Reversing evolution: re-establishing obligate metal ion dependence in a metal-independent KDO8P synthase. *J. Mol. Biol. 390*, 646–661.
12. Duewel, H. S., Radaev, S., Wang, J., Woodard, R. W., and Gatti, D. L. (2001) Substrate and metal complexes of 3-deoxy-D-manno-octulosonate 8-phosphate synthase from *Aquifex aeolicus* at 1.9 Å resolution: implications for the condensation mechanism. *J. Biol. Chem. 276*, 8393–8402.
13. Oliynyk, Z., Briseno-Roa, L., Janowitz, T., Sondergeld, P., and Fersht, A. R. (2004) Designing a metal-binding site in the scaffold of *Escherichia coli* KDO8PS. *Protein Eng. Des. Sel. 17*, 383–390.
14. Li, J., Wu, J., Fleischhacker, A. S., and Woodard, R. W. (2004) Conversion of *Aquifex aeolicus* 3-deoxy-D-manno-octulosonate 8-phosphate synthase, a metalloenzyme, into a nonmetalloenzyme. *J. Am. Chem. Soc. 126*, 7448–7449.
15. Shulami, S., Furdui, C., Adir, N., Shoham, Y., Anderson, K. S., and Baasov, T. (2004) A reciprocal single mutation affects the metal requirement of 3-deoxy-D-manno-2-octulosonate-8-phosphate (KDO8P) synthases from *Aquifex pyrophilus* and *Escherichia coli*. *J. Biol. Chem. 279*, 45110–45120.
16. Kaustov, L., Kababya, S., Du, S., Baasov, T., Gropper, S., Shoham, Y., and Schmidt, A. (2000) Structural and mechanistic investigation of 3-deoxy-D-manno-octulosonate-8-phosphate synthase by solid-state REDOR NMR. *Biochemistry 39*, 14865–14876.
17. Furdui, C., Zhou, L., Woodard, R. W., and Anderson, K. S. (2004) Insights into the mechanism of 3-deoxy-D-arabino-heptulosonate 7-phosphate synthase (Phe) from *Escherichia coli* using a transient kinetic analysis. *J. Biol. Chem. 279*, 45618–45625.
18. Furdui, C. M., Sau, A. K., Yaniv, O., Belakhov, V., Woodard, R. W., Baasov, T., and Anderson, K. S. (2005) The use of (*E*)- and (*Z*)-phosphoenol-3-fluoropyruvate as mechanistic probes reveals significant differences between the active sites of KDO8P and DAHP synthases. *Biochemistry 44*, 7326–7335.
19. Sau, A. K., Li, Z., and Anderson, K. S. (2004) Probing the role of metal ions in the catalysis of *Helicobacter pylori* 3-deoxy-D-manno-octulosonate-8-phosphate synthase using a transient kinetic analysis. *J. Biol. Chem. 279*, 15787–15794.
20. Shumilin, I. A., Bauerle, R., Wu, J., Woodard, R. W., and Kretsinger, R. H. (2004) Crystal structure of the reaction complex of 3-deoxy-D-arabino-heptulosonate-7-phosphate synthase from *Thermotoga maritima* refines the catalytic mechanism and indicates a new mechanism of allosteric regulation. *J. Mol. Biol. 341*, 455–466.
21. Du, S., Plat, D., Belakhov, V., and Baasov, T. (1997) First non-enzymatic synthesis of Kdo8P through a mechanism similar to that suggested for the enzyme Kdo8P synthase. *J. Org. Chem. 62*, 794–804.
22. Wang, J., Duewel, H. S., Stuckey, J. A., Woodard, R. W., and Gatti, D. L. (2002) Function of His185 in *Aquifex aeolicus* 3-deoxy-D-manno-octulosonate 8-phosphate synthase. *J. Mol. Biol. 324*, 205–214.
23. Howe, D. L., Sundaram, A. K., Wu, J., Gatti, D. L., and Woodard, R. W. (2003) Mechanistic insight into 3-deoxy-D-manno-octulosonate-8-phosphate synthase and 3-deoxy-D-arabino-heptulosonate-7-phosphate synthase utilizing phosphorylated monosaccharide analogues. *Biochemistry 42*, 4843–4854.
24. Hedstrom, L., and Abeles, R. (1988) 3-Deoxy-D-manno-octulosonate-8-phosphate synthase catalyzes the C-O bond cleavage of phosphoenolpyruvate. *Biochem. Biophys. Res. Commun. 157*, 816–820.
25. Li, Z., Sau, A. K., Shen, S., Whitehouse, C., Baasov, T., and Anderson, K. S. (2003) A snapshot of enzyme catalysis using electrospray ionization mass spectrometry. *J. Am. Chem. Soc. 125*, 9938–9939.
26. Kona, F., Xu, X., Martin, P., Kuzmic, P., and Gatti, D. L. (2007) Structural and mechanistic changes along an engineered path from metallo to nonmetallo 3-deoxy-D-manno-octulosonate 8-phosphate synthases. *Biochemistry 46*, 4532–4544.
27. Kohen, A., Berkovich, R., Belakhov, V., and Baasov, T. (1993) Stereochemistry of KDO8P synthase. An efficient synthesis of the 3-fluoro analogs of KDO8P. *Bioorg. Med. Chem. Lett. 3*, 1577–1582.
28. Dotson, G. D., Nanjappan, P., Reily, M. D., and Woodard, R. W. (1993) Stereochemistry of 3-deoxyoctulosonate 8-phosphate synthase. *Biochemistry 32*, 12392–12397.
29. Jorgensen, W. L., Chandrasekhar, J., J., M., and Klein, M. L. (2003) Comparison of simple potential functions for simulating liquid water. *J. Chem. Phys. 79*, 926–935.
30. Duan, Y., Wu, C., Chowdhury, S., Lee, M. C., Xiong, G., Zhang, W., Yang, R., Cieplak, P., Luo, R., and Lee, T. (2003) A point-charge force field for molecular mechanics simulations of proteins based on condensed phase quantum mechanical calculations. *J. Comput. Chem. 24*, 1999–2012.
31. Ryckaert, J.-P., Ciccotti, G., and Berendsen, H. J. C. (1977) Numerical integration of the Cartesian equations of motion of a system with constraints: molecular dynamics of n-alkanes. *J. Comput. Phys. 23*, 327–341.
32. Vreven, T., Morokuma, K., Farkas, O., Schlegel, H. B., and Frisch, M. J. (2003) Geometry optimization with QM/MM, ONIOM, and other combined methods. I. Microiterations and constraints. *J. Comput. Chem. 24*, 760–769.

33. Vreven, T., Frisch, M. J., Kudin, K. N., Schlegel, H. B., and Morokuma, K. (2006) Geometry optimization with QM/MM methods II: Explicit quadratic coupling. *Mol. Phys. 104*, 701–714.
34. Vreven, T., Byun, K. S., Komaromi, I., Dapprich, S., Montgomery, J. A., Jr., Morokuma, K., and Frisch, M. J. (2006) Combining quantum mechanics methods with molecular mechanics methods in ONIOM. *J. Chem. Theory Comput. 2*, 815–826.
35. Halgren, T. A., and Lipscomb, W. N. (1977) The synchronous-transit method for determining reaction pathways and locating molecular transition states. *Chem. Phys. Lett. 49*, 225–232.
36. Jensen, A. (1983) Location of transition states and stable intermediates by MINIMAX/MINIMI optimization of synchronous transit pathways. *Theor. Chim. Acta 63*, 269–290.
37. Bell, S., and Crighton, J. S. (1984) Locating transition states. *J. Chem. Phys. 80*, 2464–2475.
38. Warshel, A., and Parson, W. W. (2001) Dynamics of biochemical and biophysical reactions: insight from computer simulations. *Q. Rev. Biophys. 34*, 563–679.
39. Warshel, A., Sharma, P. K., Kato, M., Xiang, Y., Liu, H., and Olsson, M. H. (2006) Electrostatic basis for enzyme catalysis. *Chem. Rev. 106*, 3210–3235.
40. Weinhold, F. (1988) Natural bond orbital methods, in Encyclopedia of Computational Chemistry (Schleyer, P. v. R., , N. L. A., Clark, T., Gasteiger, J., Kollman, P. A., Schaefer, H. F., III, and Schreiner, P. R., Eds.) pp 1792−1811, John Wiley & Sons, Chichester, U.K.
41. Ahn, M., Pietersma, A. L., Schofield, L. R., and Parker, E. J. (2005) Mechanistic divergence of two closely related aldol-like enzyme-catalysed reactions. *Org. Biomol. Chem. 3*, 4046–4049.
42. Evans, M. G., and M., P. (1935) Some applications of the transition state method to the calculation of reaction velocities, especially in solution. *Trans. Faraday Soc. 31*, 875–894.
43. Gladstone, S., Laidler, K. J., Eyring, H. (1941) The Theory of Rate Processes , McGraw-Hill, New York and London.
44. Neria, E., and Karplus, M. (1997) Molecular dynamics of an enzyme reaction: proton transfer in TIM. *Chem. Phys. Lett. 267*, 23–30.
45. Billeter, S. R., Webb, S. P., Agarwal, P. K., Iordanov, T., and Hammes-Schiffer, S. (2001) Hydride transfer in liver alcohol dehydrogenase: quantum dynamics, kinetic isotope effects, and role of enzyme motion. *J. Am. Chem. Soc. 123*, 11262–11272.
46. Nam, K., Prat-Resina, X., Garcia-Viloca, M., Devi-Kesavan, L. S., and Gao, J. (2004) Dynamics of an enzymatic substitution reaction in haloalkane dehalogenase. *J. Am. Chem. Soc. 126*, 1369–1376.
47. Pu, J., Gao, J., and Truhlar, D. G. (2006) Multidimensional tunneling, recrossing, and the transmission coefficient for enzymatic reactions. *Chem. Rev. 106*, 3140–3169.
48. Page, M. I., and Jencks, W. P. (1971) Entropic contributions to rate accelerations in enzymic and intramolecular reactions and the chelate effect. *Proc. Natl. Acad. Sci. U.S.A. 68*, 1678–1683.
49. Jencks, W. P. (1975) Binding energy, specificity, and enzymic catalysis: the circe effect. *Adv. Enzymol. Relat. Areas Mol. Biol. 43*, 219–410.
50. Snider, M. J., Gaunitz, S., Ridgway, C., Short, S. A., and Wolfenden, R. (2000) Temperature effects on the catalytic efficiency, rate enhancement, and transition state affinity of cytidine deaminase, and the thermodynamic consequences for catalysis of removing a substrate "anchor". *Biochemistry 39*, 9746–9753.
51. Villa, J., Strajbl, M., Glennon, T. M., Sham, Y. Y., Chu, Z. T., and Warshel, A. (2000) How important are entropic contributions to enzyme catalysis? *Proc. Natl. Acad. Sci. U.S.A. 97*, 11899–11904.
52. Villa, J., and Warshel, A. (2001) Energetics and dynamics of enzymatic reactions. *J. Phys. Chem. B 105*, 7887–7907.
53. Xu, X., Kona, F., Wang, J., Lu, J., Stemmler, T., and Gatti, D. L. (2005) The catalytic and conformational cycle of *Aquifex aeolicus* KDO8P synthase: role of the L7 loop. *Biochemistry 44*, 12434–12444.
54. Smith, A. J., Muller, R., Toscano, M. D., Kast, P., Hellinga, H. W., Hilvert, D., and Houk, K. N. (2008) Structural reorganization and preorganization in enzyme active sites: comparisons of experimental and theoretically ideal active site geometries in the multistep serine esterase reaction cycle. *J. Am. Chem. Soc. 130*, 15361–15373.
55. Benkovic, S. J., Hammes, G. G., and Hammes-Schiffer, S. (2008) Free-energy landscape of enzyme catalysis. *Biochemistry 47*, 3317–3321.